Tectonophysics 494 (2010) 138–148

Contents lists available at ScienceDirect

Tectonophysics

journal homepage: www.elsevier.com/locate/tecto

Two anisotropic layers in central orogenic belt of North China Craton

Ling Bai *, Hitoshi Kawakatsu, Yuichi Morita

Earthquake Research Institute, University of Tokyo, 1-1-1 Yayoi, Bunkyo-ku, Tokyo 113-0032, Japan

ARTICLE INFO

Article history:
Received 31 August 2009
Received in revised form 21 July 2010
Accepted 6 September 2010
Available online 16 September 2010

Keywords:
Two layers of anisotropy
North China Craton
Shear-wave splitting

ABSTRACT

We present evidence of two layers of anisotropy in Earth's upper mantle beneath the central orogenic belt of the North China Craton from teleseismic shear-wave splitting analysis. A one-layer model is in disagreement with the well-constrained azimuth-dependent splitting parameters for stations in the central orogenic belt; however, two layers of anisotropy improve the fit to the data. At the bottom layer, the fast polarization directions are subparallel to the absolute plate motion, indicating the presence of the current strain within the subcratonic asthenosphere related to the interactions between the surrounding plates. In contrast, at the top layer, the fast polarization directions are consistent with the strikes of the local surface faults, confirming a combined contribution of the past orogenies in the lithosphere.

1. Introduction

The effect of anisotropy on seismic waves has been extensively studied to understand the tectonic and geodynamic processes in Earth. In the shallow crust, anisotropy may be caused by preferentially aligned cracks or by layered bedding in sedimentary formations. At depths where cracks close due to high pressure, anisotropy is normally associated with crystals aligned along the mantle flow direction. The upper mantle beneath the Moho is a primary source of anisotropic signals. As a nearly vertical ray path of a seismic wave is usually required for detecting anisotropy, constraining the source depth is rather difficult. Commonly, strategies for resolving the depth-dependent anisotropic structure use observational datasets of seismic waves generated by earthquakes at well-distributed azimuths (Silver and Savage, 1994). Most previous studies provided limited azimuthal coverage and did not allow the detection of the complex upper mantle, even for a minimal two-layer model.

Recent studies have provided important clues for the detection of two anisotropic layers. First, Silver and Savage (1994) derived expressions for the interpretation of splitting parameters in more complex media. They showed that several stations along the San Andreas fault zone exhibit the properties of two layers, with the top layer being parallel to the local strike of the fault. Snyder et al. (2003) observed an increasing trend in the delay time as a function of the earthquake azimuth at the Slave Craton in Canada. The upper layer is hypothesized to be within the uppermost mantle and the crust, and the lower layer is probably within the mantle.

In this study, we present evidence of two layers of anisotropy in a cratonic upper mantle of the Earth. Shear-wave splitting of the SKS, SKKS, PKS, and S phases for 68 teleseismic events is measured to investigate the tectonic process and deep structures beneath the North China Craton. We deployed four broadband seismographs in and around the North China Craton during a period between October 1999 and November 2003. The data obtained from two IRIS stations, which have been operational for over ten years, are also analyzed. Splitting analysis carried out using the new data provides more detailed constrains on the interpretation of the tectonic evolution process in North China.

2. Tectonic setting

Mainland China is located in the southeastern part of the Eurasia Plate, and it is surrounded by four major tectonic plates, namely, the Indian, Philippine Sea, Pacific, and North American Plates (Fig. 1(a)). The three oldest cratons in the mainland China are the North China Craton (NCC, also called the Chinese part of the Sino-Korean Craton), Yangtze Craton, and Tarim Craton. The NCC has an area of approximately 1.7 million km^2 and it covers Northeastern China, Inner Mongolia, and the Yellow Sea. The tectonic and geodynamic evolution processes of the NCC have attracted much attention because the NCC has a rather unique crust and mantle structure as compared to other ancient continental nuclei. The NCC is tectonically divided into an eastern block (EB) and a western block (WB) by a north–south (NS) trending central orogenic belt (COB) (Fig. 1(b)) (e.g., Kusky and Li, 2003). The WB, also called the Ordos Block, is a stable craton with a thick mantle root and a lack of internal deformation since the Precambrian; only a few earthquakes occur here. In contrast, the EB, also called the North China Basin, is atypical for a craton in that it exhibits active seismicity (e.g., the 1966 Xingtai earthquake of M7.2, the 1975 Haicheng earthquake of M7.3, and the 1976 Tangshang earthquake of M7.8) (Earthquake Defence Department, China Earthquake Administration, 1999), and it has a thin lithosphere reflecting

* Corresponding author. Present address: Geological Sciences, University of Michigan, 1100 N. University Ave., Ann Arbor, MI, USA. Fax: +1 734 763 4690.
E-mail address: lingb@umich.edu (L. Bai).

0040-1951/$ – see front matter © 2010 Elsevier B.V. All rights reserved.
doi:10.1016/j.tecto.2010.09.002

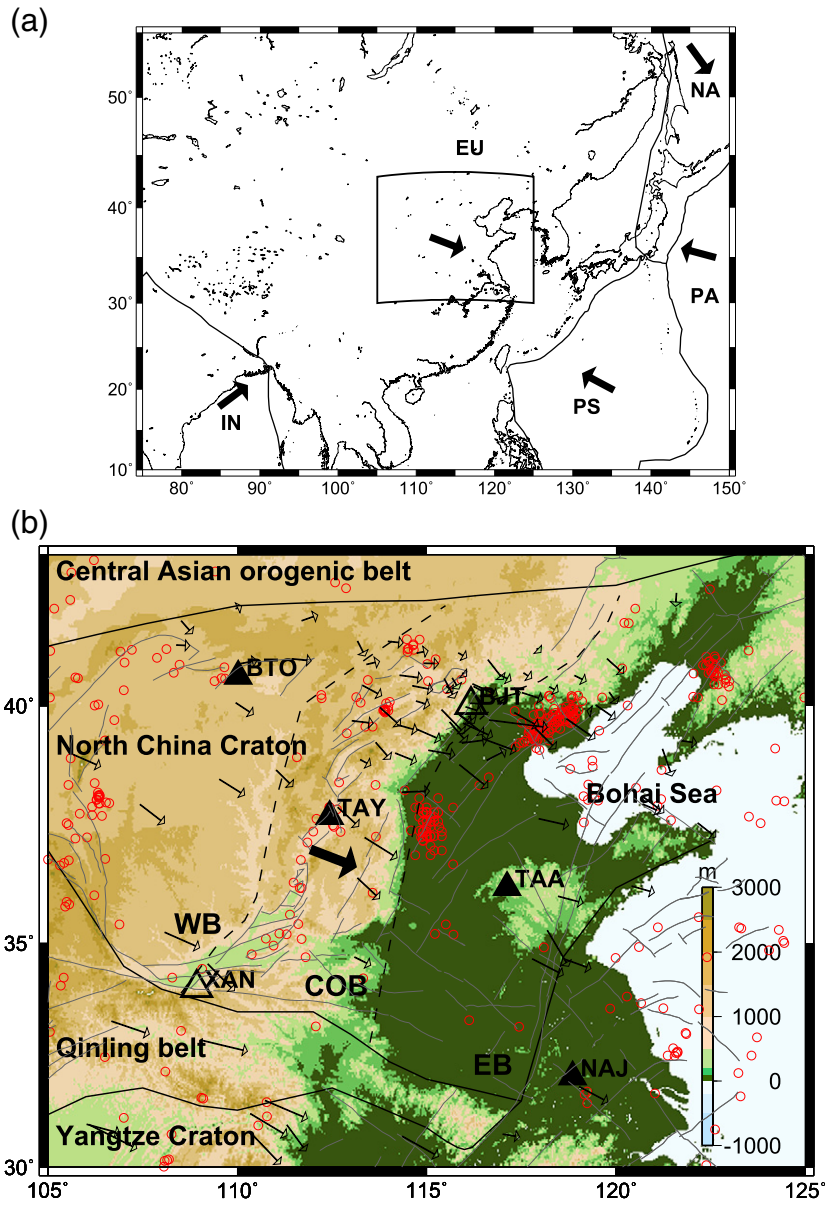

Fig. 1. (a) Study area (rectangle) located at the junction of five major plates, namely, the Indian (IN), Eurasian (EU), Philippine Sea (PS), Pacific (PA), and North American (NA) Plates. Thick lines indicate plate boundaries. Arrows indicate the absolute plate movement of major plates obtained using the GSRM v1.2 model. (b) Locations of four temporary stations (solid triangles) and two IRIS stations (open triangles) used in this study. Black solid lines indicate boundaries of tectonic units and dotted lines are boundaries between the western block (WB), central orogenic belt (COB), and eastern block (EB). Gray solid lines are active faults (Deng et al., 2003). Red circles indicate earthquakes ($M \geq 4$; depth ≤ 100 km) between 1964/01/01–2004/12/12 referred from the NEIC PDE catalog. The thick arrow indicates the averaged absolute plate motion of the Eurasia Plate by considering several models of plate motion. Thin arrows indicate the GPS station velocities relative to the stable Eurasia (Wang et al., 2001). The background indicates the topography.

the lack of a thick mantle root (e.g., Huang et al., 2003). In the past, the COB has undergone high-grade regional metamorphism; this, in turn, has led to the final uplift of the metamorphic terrain at several Ga (Kusky and Li, 2003).

3. Data and methodology

We deployed four broadband seismographs (Guralp CMG-3T) in and around the NCC during a period between October 1999 and November 2003 as a part of the Ocean Hemisphere network Project (OHP; http://eri-ndc.eri.utokyo.ac.jp) (solid triangles in Fig. 1(b)) (Morita et al., 1999). These seismographs were deployed to study the deep structure of Earth as well as to study the regional structure in and around the NCC. The four temporary stations, called BTO (Baotou, Inner Mongolia), TAY (Taiyuan, Shanxi Province), TAA (Taian, Shandong Province), and NAJ (Nanjing, Jiangsu Province), are located at the WB, COB, EB, and Yangtze Craton, respectively. We supplement the temporary data with those obtained from two nearby IRIS stations, BJT and XAN, which have been operational as FDSN seismic stations since May 1994 and May 1995, respectively. To investigate the seismic anisotropy beneath the stations, we selected clear recordings of the teleseismic SKS phase at epicentral distances of 85°–120°, SKKS at 100°–130°, PKS at 120°–150°, and S at 30°–80°. The use of P-S converted phases at the core–mantle boundary and S phase from deep earthquakes ensured that the observed anisotropy is mainly from the receiver side. We selected 68 events for which data with a high signal-to-noise ratio and splitting parameters with small errors were available. All 68 events are shown in Fig. 2 and also listed in Table 1.

When a seismic wave propagates through an anisotropic medium, two shear waves with different polarizations will have different

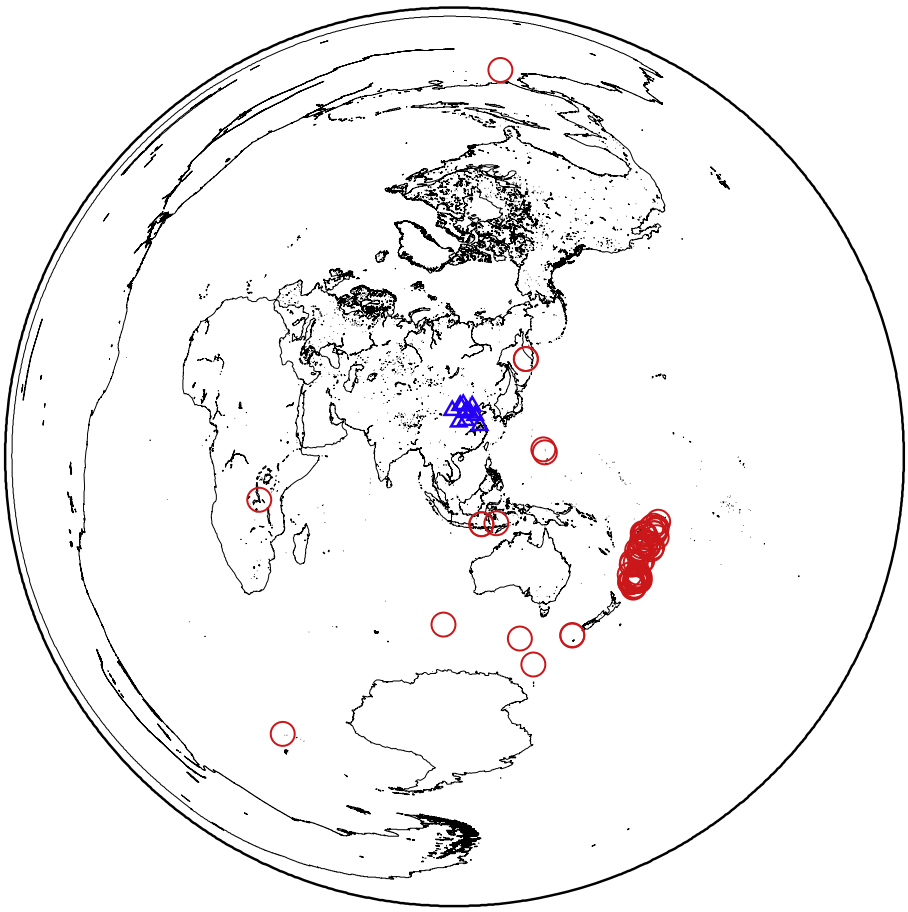

Fig. 2. 68 events for which splitting parameters with small errors were available (open circles). Triangles indicate the four temporary stations and two IRIS stations.

velocities. We initially assume that the anisotropy is located within a single homogeneous layer. In this case, the splitting parameters will be independent of the incoming polarization angle of a seismic wave. To determine the fast polarization direction (FPD, φ) and the delay time (δt) between the fast and slow components, we use the shear-wave splitting method proposed by Silver and Chan (1991) for individual earthquakes. A grid search over possible values is performed to linearize the shear-wave particle motion when the effect of the anisotropy is removed. Fig. 3 shows examples of waveform splitting for data obtained from the TAY and TAA stations. All records are band-pass filtered between 0.02 and 1.0 Hz to reduce the background noise. The master time windows used are 10–15 s around the phases of interest based on the predicted travel times obtained from the IASP91 model (Kennett and Engdahl, 1991). The arrival times of all phases listed in this model are indicated on the waveforms to ensure no contamination from other phases in the analysis. After these measurements of the splitting parameter for each event, the splitting parameter for each station is derived by stacking. We use the multi-event stacking procedure described by Wolfe and Silver (1998) to stack the error surface of individual earthquakes and reduce the uncertainty in the estimation of φ and δt at each station. In this study, only good measurements that satisfy the following conditions are used to constrain the final result (Bai et al., 2009): (1) signal-to-noise ratios (SNR) are large (SNR$\geq$4); (2) The 95% confidence regions of the estimated splitting parameters are small ($2\sigma\varphi<22.5°$, $2\sigma\delta t<1.0$ s). All our data satisfy the condition that the back azimuth (BAZ) separation from the fast or slow polarization directions is larger than 10°. As described in a later section, the assumption of a single-layer model appears to have been violated for stations in the COB area. We then apply a method proposed by Silver and Savage (1994) to test a multiple-layer anisotropic model. When a seismic wave propagates through two homogeneous layers, the signal is split twice. We try to find the best solutions for four splitting parameters [(φ1, δt1), (φ2, δt2)] for the bottom and top layers, respectively. A grid search with a step size of 1° for the FPD and 0.1 s for the delay time is performed.

4. Splitting results

4.1. Parameters for a single-layer model

We measure a total of 81 apparent splitting parameters from the SKS, SKKS, PKS, and S phases. The splitting parameters of individual records with 2σ uncertainties determined from the 95% confidence interval in the (φ–δt) domain are listed in Table 2. Fig. 4 shows the FPDs and delay times as a function of the BAZs. The result of the final station splitting parameters derived by stacking are presented in the main panel of Fig. 5 and Table 3.

The BJT (Baijiatuan, Beijing City) station is located at the eastern margin of the mountain belts and northwest of the Phanerozoic North China Basin. The orientations of the regional surface faults trend northeast. For this station, differing SKS splitting results have been reported previously, including (1) ($104\pm8.3°$, 0.9 ± 0.11 s) using 30 events (Luo et al., 2004), (2) ($112\pm10°$, 0.8 ± 0.3 s) using 35 events (Liu et al., 2008), (3) (110°, 0.8 s) using 5 events (Liu et al., 2001), (4) ($59\pm16°$, 0.86 ± 0.48 s) using 6 events (Zhao et al., 2007), and

Table 1
Selected events.

Event ID	Data	Time	λE/°	φN/°	H/km	MW/(Me)	Observation no.
96111230	1996/04/20	23:03:29.71	−179.6920	−22.2930	592.60	5.70	1
97078174	1997/03/19	17:50:42.27	−173.8980	−16.6100	98.90	5.80	1
97245121	1997/09/02	12:13:22.92	−75.7490	3.8490	198.70	(6.80)	1
97281104	1997/10/08	10:47:49.92	178.3550	−29.2500	617.30	5.70	1
97360053	1997/12/26	05:34:24.71	−179.6900	−22.3380	588.40	5.90	1
98136022	1998/05/16	02:22:03.21	−179.5190	−22.2270	586.10	(6.90)	1
99099121	1999/04/09	12:16:01.89	178.2210	−26.3540	621.20	6.20	1
99103103	1999/04/13	10:38:48.40	−176.4600	−21.4220	164.20	(6.80)	1
99253193	1999/09/10	19:37:44.81	−178.2700	−32.8310	33.00	6.00	1
00001055	2000/01/01	05:58:19.78	153.6700	−60.7220	10.00	6.00	1
00008164	2000/01/08	16:47:20.58	−174.2480	−16.9250	183.40	(7.20)	1
00013200	2000/01/13	20:07:14.44	−178.7420	−17.6100	535.00	6.20	2
00016150	2000/01/16	15:00:40.84	−178.1330	−30.2380	33.00	5.90	1
00026132	2000/01/26	13:26:50.00	−174.0020	−17.2720	33.00	(6.30)	1
00046020	2000/02/15	02:05:00.51	145.4010	17.6750	521.50	(5.90)	1
00109172	2000/04/18	17:28:12.39	−176.4690	−20.6640	220.70	(6.00)	2
00125203	2000/05/04	20:36:32.48	−178.5220	−17.9140	515.80	(6.50)	1
00129213	2000/05/08	21:35:42.85	179.8390	−31.3190	383.10	5.60	3
00166021	2000/06/14	02:15:25.84	178.0460	−25.5160	604.60	(6.40)	2
00168202	2000/06/16	20:23:33.36	−178.4640	−28.8760	222.60	5.60	1
00215003	2000/08/02	00:37:16.32	−174.8200	−17.9450	191.20	5.60	1
00220143	2000/08/07	14:33:55.91	123.3570	−7.0180	648.50	(6.50)	1
00228042	2000/08/15	04:30:08.80	179.7250	−31.5110	357.70	(6.60)	2
00230000	2000/08/17	00:04:29.15	−174.7710	−21.9010	33.00	5.80	1
00276022	2000/10/02	02:25:31.31	30.7090	−7.9770	34.00	(6.50)	1
00353011	2000/12/18	01:19:21.65	−179.1240	−21.1780	628.20	6.60	1
01038151	2001/02/07	15:16:15.22	153.8480	52.7510	426.60	5.70	2
01047055	2001/02/16	05:59:09.48	117.4880	−7.1610	521.00	6.10	2
01070005	2001/03/11	00:50:40.49	−177.9660	−25.3730	231.00	5.80	4
01127000	2001/05/07	00:00:37.54	−173.4680	−14.9270	33.00	5.70	1
01143153	2001/05/23	15:35:23.17	−178.7030	−17.7080	567.20	5.60	1
01146105	2001/05/26	10:57:26.15	−177.8420	−20.2920	406.50	6.40	1
01154024	2001/06/03	02:41:57.16	−178.6330	−29.6660	178.10	7.20	1
01258150	2001/09/15	15:04:34.08	−175.0100	−22.3930	10.00	6.00	1
01309230	2001/11/05	23:07:11.72	−179.2510	−17.2890	564.10	6.30	1
01326041	2001/11/22	04:17:26.64	−176.7240	−31.0680	33.00	5.80	2
02007132	2002/01/07	13:26:26.48	144.9580	18.9570	599.40	5.90	1
02068122	2002/03/09	12:27:11.22	−27.3320	−56.0190	118.40	6.00	1
02128052	2002/05/08	05:26:00.36	−174.5730	−17.9480	130.80	6.20	1
02165063	2002/06/14	06:35:17.23	101.8910	−47.2150	10.00	5.50	2
02167065	2002/06/16	06:55:13.28	−178.6960	−17.8660	569.00	5.90	1
02181212	2002/06/30	21:29:36.30	179.2500	−22.2010	620.40	6.50	2
02225141	2002/08/13	14:13:54.99	−177.3670	−30.7720	33.00	5.60	1
03004051	2003/01/04	05:15:03.84	−177.6610	−20.5700	378.00	6.50	2
03124131	2003/05/04	13:15:18.66	−178.2320	−30.5310	62.40	6.70	1
03124200	2003/05/04	20:08:46.48	−178.2900	−30.5870	45.60	6.40	1
03156082	2003/06/05	08:23:17.44	−178.8040	−30.6180	115.20	5.80	1
04011080	2004/01/11	08:07:04.96	−176.1750	−16.2370	366.10	5.90	1
04043134	2004/02/12	13:47:32.62	−173.5180	−19.2260	21.20	5.80	1
04067150	2004/03/07	15:04:51.12	−178.2960	−32.5270	10.00	5.80	1
04127151	2004/05/06	15:16:22.34	−175.0710	−15.7590	267.00	5.70	1
05078173	2005/03/19	17:34:46.18	−179.5470	−21.8930	598.70	6.30	1
06055141	2006/02/24	14:15:45.21	−179.5900	−17.9950	622.40	6.10	1
06320202	2006/11/16	20:29:54.97	139.4730	−51.9960	10.00	6.10	1
07126215	2007/05/06	22:01:08.92	−179.3150	−19.4060	688.00	6.10	1
07268051	2007/09/25	05:16:01.12	179.9980	−30.9650	416.70	6.20	1
07273094	2007/09/30	09:47:51.97	164.1100	−49.1380	18.00	6.60	1
07289210	2007/10/16	21:05:43.27	179.5300	−25.7750	509.30	6.60	1
08117233	2008/04/26	23:34:49.39	164.1170	−49.0910	10.00	6.10	1
08185030	2008/07/03	03:02:37.56	−179.7780	−23.3700	581.20	6.20	1
08198170	2008/07/16	17:09:19.07	−178.5060	−31.1310	89.00	5.50	1
08273151	2008/09/29	15:19:31.59	−177.6830	−29.7560	36.00	7.00	1
08279091	2008/10/05	09:12:36.07	−177.1760	−30.1840	10.00	6.20	1
08334055	2008/11/29	05:59:16.58	−177.7160	−18.7010	386.00	6.00	1
08344062	2008/12/09	06:23:59.75	−176.9240	−31.2320	18.00	6.80	1
09043185	2009/02/12	18:54:28.18	−178.1110	−31.2320	23.80	5.80	1
09230212	2009/08/18	21:20:47.55	−178.3910	−26.0640	269.80	6.30	1
09326224	2009/11/22	22:47:27.48	179.4670	−31.5690	435.70	6.20	2

(5) (73.33 ± 3.08°, 0.29 ± 0.17 s) using 9 events (Iidaka and Niu, 2001). Our stacked results (109 – 3° and 109 + 2°, 0.78 – 0.08 s and 0.78 + 0.12 s) obtained from 23 high-quality measurements are in good agreement with those of the first three studies mentioned above. Remarkable variations of the apparent FPD from 40° to 120° and of the delay time from 0.35 s to 1.5 s at a back-azimuthal range of 115° to

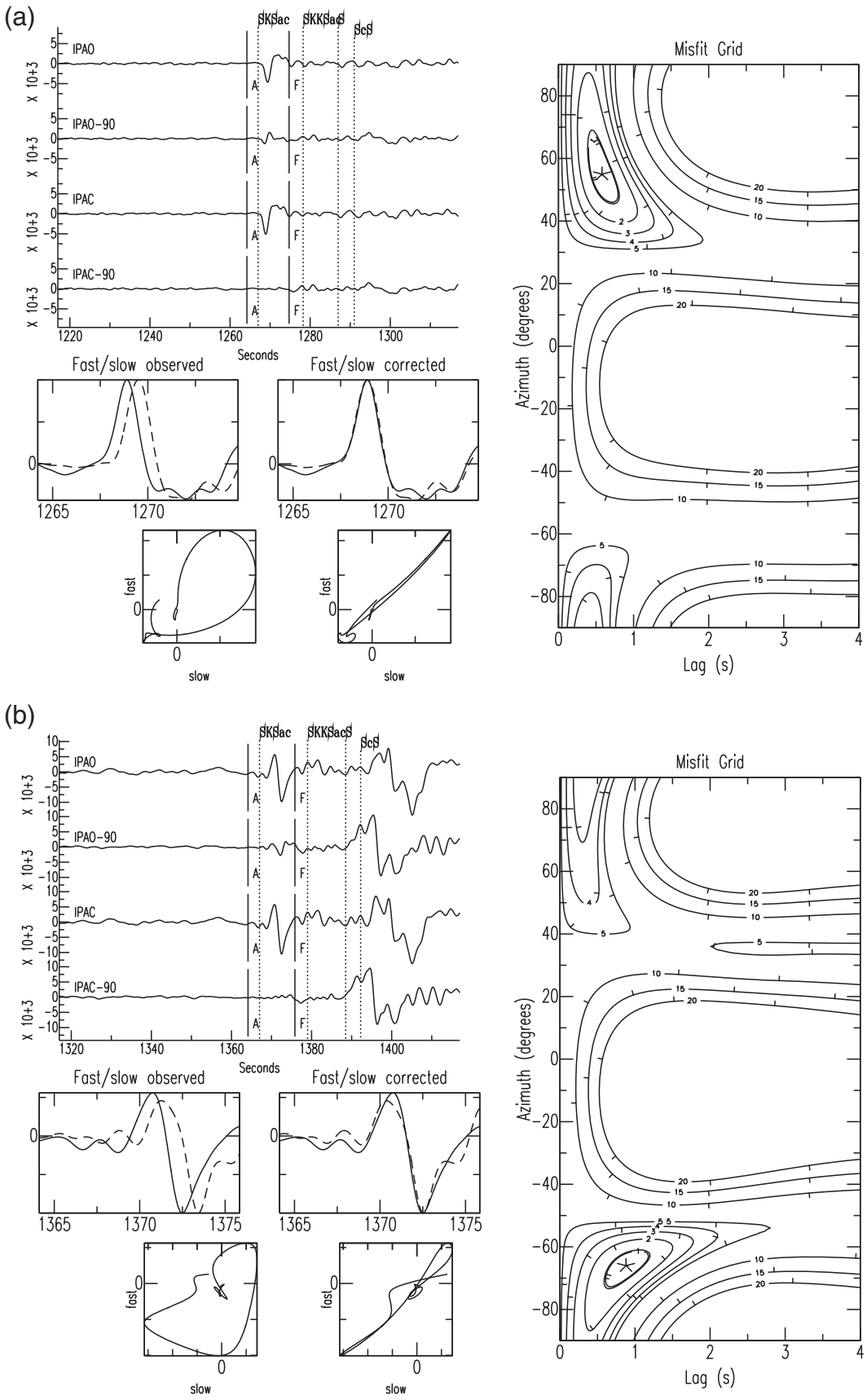

Fig. 3. Examples of shear-wave splitting analysis from (a) TAY station for event 003530119 and (b) TAA station for event 011540240. Upper left: recorded radial and transverse components of the original waveforms (IPAO, IPAO-90°) and anisotropy-corrected waveforms (IPAC, IPAC-90°) (IPAO: observed incident polarization azimuth, IPAC: corrected incident polarization azimuth.). Dashed lines indicate phase arrival times predicted using IASP91. Vertical solid lines indicate the selected time window between A and F during which splitting measurements are carried out. Lower left: observed and corrected fast (solid line) and slow (dashed line) waves and corresponding horizontal particle motion. Right: misfit grid shows the 95% confidence region (double contour) and the optimum φ and δt (asterisk).

Table 2
Summary of SKS measurements.

Station	Event ID	ϕ/°	2 $\sigma\phi$/°	δt/s	2 $\sigma\delta t$/s	BAZ/°	Phase
BTO	02128052	−23	21.5	0.86	0.31	112.9	SKS
	02167065	−15	19.5	0.90	0.39	115.5	SKS
	03004051	−24	22.0	0.98	0.49	116.8	SKS
	01047055	−51	6.5	1.36	0.23	170.0	S
TAY	00013200	59	13.0	0.56	0.18	116.8	SKS
	00046020	47	15.0	0.50	0.27	115.5	S
	00109172	48	12.0	0.82	0.51	117.6	SKS
	00125203	61	14.5	0.56	0.17	116.8	SKS
	00129213	62	11.5	0.98	0.48	127.7	SKS
	00166021	61	13.5	0.80	0.32	124.6	SKS
	00215003	42	22.0	0.48	0.34	114.5	SKS
	00220143	37	8.0	1.04	0.16	164.8	S
	00228042	55	7.0	1.10	0.40	127.9	SKS
	00230000	52	12.5	0.64	0.24	117.5	SKS
	00353011	55	11.5	0.58	0.20	119.6	SKS
	01038151	87	21.0	0.72	0.37	48.8	S
	01047055	45	19.0	0.60	0.25	172.9	S
	01070005	59	10.5	0.72	0.23	122.0	SKS
	01146105	54	21.5	0.76	0.47	118.2	SKS
	01309230	61	17.0	0.56	0.20	116.8	SKS
	01326041	52	10.5	1.24	0.67	125.5	SKS
	02007132	42	18.0	0.28	0.21	114.3	S
	02165063	57	21.5	0.66	0.32	187.2	SKS
	02167065	55	10.0	0.56	0.15	116.9	SKS
	02181212	54	17.0	0.80	0.47	121.4	SKS
	03004051	59	22.0	0.46	0.29	118.3	SKS
N	00016150	−76	17.5	1.30	0.72	128.5	SKS
	00166021	−68	6.5	0.90	0.29	127.4	SKS
	00168202	−66	6.5	1.34	0.52	127.7	SKS
	01038151	−75	8.5	0.74	0.16	45.6	S
	01070005	−67	21.5	0.72	0.58	124.8	SKS
	01154024	−66	4.0	0.90	0.22	128.4	SKS
NAJ	00129213	−87	11.5	1.46	0.49	131.3	SKS
	02068122	67	13.0	0.70	0.23	214.4	SKKS
BJT	97245121	−52	7.0	1.00	0.28	16.9	PKS
	97281104	86	13.0	0.82	0.24	129.4	SKS
	99099121	−73	8.0	0.82	0.42	127.5	SKS
	99253193	−71	9.0	0.82	0.54	129.7	SKS
	00129213	−70	6.0	0.76	0.24	129.9	SKS
	00228042	−61	4.0	1.06	0.58	130.1	SKS
	00276022	−83	15.0	1.54	0.76	261.0	SKS
	01070005	90	22.0	0.36	0.18	124.3	SKS
	01326041	−71	10.0	0.76	0.66	127.6	SKS
	02225141	80	22.0	0.64	0.27	127.8	SKS
	03124131	−74	16.0	0.80	0.80	128.1	SKS
	03124200	−70	7.0	1.36	0.74	128.2	SKS
	04043134	41	14.5	0.84	0.58	117.1	SKS
	04067150	−63	10.0	0.98	0.99	129.6	SKS
	05078173	−86	14.0	0.50	0.32	123.0	SKS
	07126215	57	19.5	0.44	0.23	121.1	SKS
	07268051	−87	22.0	0.62	0.34	129.5	SKS
	08117233	−56	14.0	0.84	0.44	150.4	SKS
	08185030	67	21.5	0.38	0.16	124.1	SKS
	08273151	75	22.0	0.70	0.38	127.2	SKS
	08344062	−64	8.0	1.04	0.95	127.8	SKS
	09043185	85	20.5	0.84	0.31	128.5	SKS
	09326224	−74	9.5	1.10	0.36	130.3	SKS
XAN	96111230	−89	8.0	1.42	0.40	118.6	SKS
	97078174	90	6.0	1.36	0.28	110.8	SKS
	97142074	−80	8.0	1.68	0.47	33.8	SKKS
	97360053	−88	5.0	1.38	0.26	118.6	SKS
	98136022	89	11.0	1.32	0.44	118.4	SKS
	99103103	81	20.0	1.00	0.41	116.1	SKS
	00001055	88	16.0	1.20	0.60	159.3	SKS
	00008164	−88	12.0	1.22	0.84	111.2	SKS
	00013200	82	8.0	1.30	0.20	114.3	SKS
	00026132	82	10.0	1.12	0.38	111.4	SKS
	00109172	−86	9.0	1.22	0.64	115.5	SKS
	01070005	−86	7.0	1.28	0.32	120.0	SKS
	01127000	67	12.0	0.84	0.16	109.2	SKS
	01143153	85	9.0	1.32	0.32	114.4	SKS
	01258150	−83	9.0	1.28	0.70	116.0	SKS
	02181212	−88	16.0	1.32	0.64	119.1	SKS
	02211065	−82	9.5	1.28	0.29	218.2	PKS
	03156082	−85	4.0	0.70	0.08	124.6	SKS
	04011080	89	8.0	1.50	0.48	111.8	SKS
	04127151	−89	4.0	1.54	0.26	110.7	SKS
	06055141	90	7.0	1.36	0.24	115.1	SKS
	06320202	−73	22.0	1.16	0.66	161.7	SKS
	07273094	−65	19.0	1.16	0.84	147.2	SKS
	07289210	−82	7.0	1.26	0.32	121.7	SKS
	08198170	−76	7.0	1.88	0.56	124.9	SKS
	08279091	−72	8.0	1.96	0.98	123.4	SKS
	08334055	89	9.0	1.42	0.36	114.6	SKS
	09230212	−80	4.5	1.30	0.23	120.8	SKS
	09326224	−75	13.0	0.82	0.39	126.3	SKS

130° are found for the BJT station (Fig. 4). The large variations in the measurements obtained by different studies might have resulted from the use of a limited number of events.

The XAN (Xi'an, Shaanxi Province) station is located at the boundary between the NCC and the Qinling belt. The results (94 ± 1°, 1.18 – 0.06 s and 1.18 + 0.08 s) obtained from 29 high-quality observations are consistent with those obtained by Luo et al. (2004) (89 ± 4.9°, 1.2 ± 0.08 s) and Liu et al. (2008) (89 ± 4°, 1.2 ± 0.2 s), but inconsistent with those obtained by Zhao et al. (2007) (35 ± 13°, 1.37 ± 1.47 s).

At the TAA station, the final results (112 – 3° and 112 + 2°, 0.86 – 0.14 s and 0.86 + 0.10 s) are obtained from six earthquakes. The splitting results at this station are consistent with those estimated by Luo et al. (2004) from eight events. The TAY station is quite far from other stations at which seismic observations have been carried out previously. Data from 22 high-quality events are analyzed to obtain the final results (54 ± 3°, 0.58 ± 0.06 s). In addition, results at the BTO (138 – 7° and 138 + 12°, 1.16 ± 0.24 s) and NAJ (83 – 20° and 83 + 21°, 0.74 ± 0.30 s) stations are obtained from four and two events, respectively.

4.2. Evidence for multiple layers of anisotropy

4.2.1. Measurements under the assumption of two layers

As mentioned in Section 4.1, small to large values of δt (0.58 s for TAY to 1.18 s for XAN) and large variation of φ (NE–SW for TAY to NW–SE for TAA) are found, indicating that the regimes of seismic anisotropy in the study area are laterally variable or/and the single layer of anisotropy that we assumed initially is too simplistic. The majority of the events used lie in Fiji and adjacent regions. However, these events provide robust and statistically distinct variations for both the FPD and delay time with respect to the initial polarization of the seismic waves, which is approximately equal to the BAZ for the phases we used. At the BJT station, well-constrained splitting parameters obtained from 20 events with SKS phases define a clear increasing trend in the FPDs over the BAZs of 115° to 130° (Fig. 6), and large variations in both the FPD and the delay time are obtained in different studies. In addition, previous studies have shown some dependence of the observed FPD on the orientation of surface faults at the COB area (Zhao and Zheng, 2005; Huang et al., 2008).

Taking these observations into account, we test a two-layer model for three stations (BJT, TAY, and XAN) in the COB area using the method proposed by Silver and Savage (1994). The misfit between the model prediction and the observed apparent splitting parameters is calculated using $Z = \Sigma((P_i - O_i)/(2\sigma)_i)^2$ ($i = 1, 2$), where Pi is the predicted parameter and Oi is the observed parameter for both the FPD ($i = 1$) and the delay time ($i = 2$), and 2σ is the 95% confidence region of the estimated FPD and delay time. To estimate the error variance, we used the bootstrap method (Efron, 1979) based on resampling. Normal-distributed resamplings of the apparent splitting parameters within the 95% confidence regions are generated and splitting parameters for the two-layer model are reestimated. 500

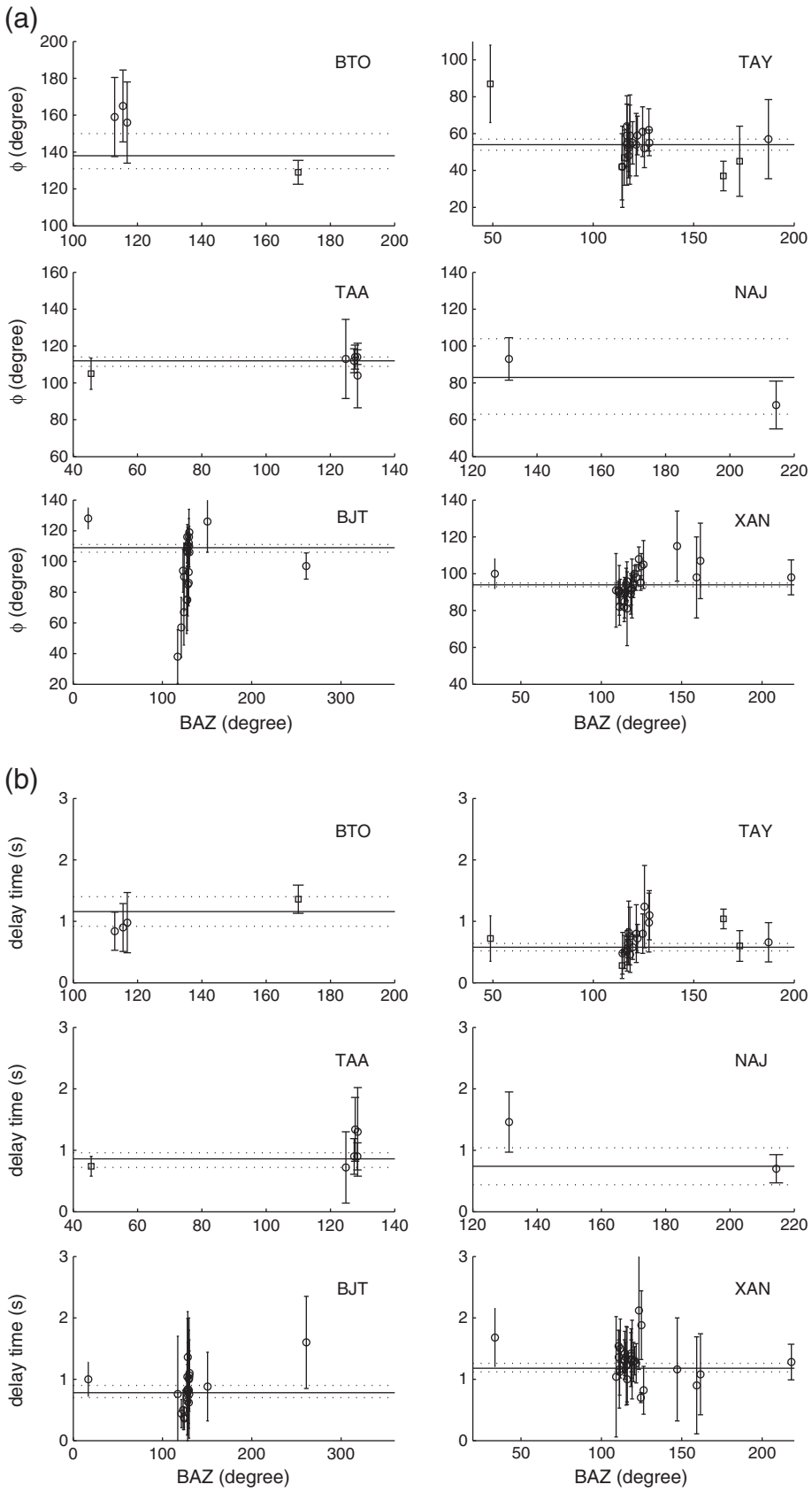

Fig. 4. Graphs with (a) FPD and (b) delay time versus BAZ. Open dots for SKS-type phases, open squares for S phase, and vertical lines indicate FPDs and delay times, and their corresponding uncertainties. Horizontal solid line and two dotted lines indicate the final splitting parameters and the -2σ and 2σ uncertainties calculated from stacking the apparent splitting measurements, respectively.

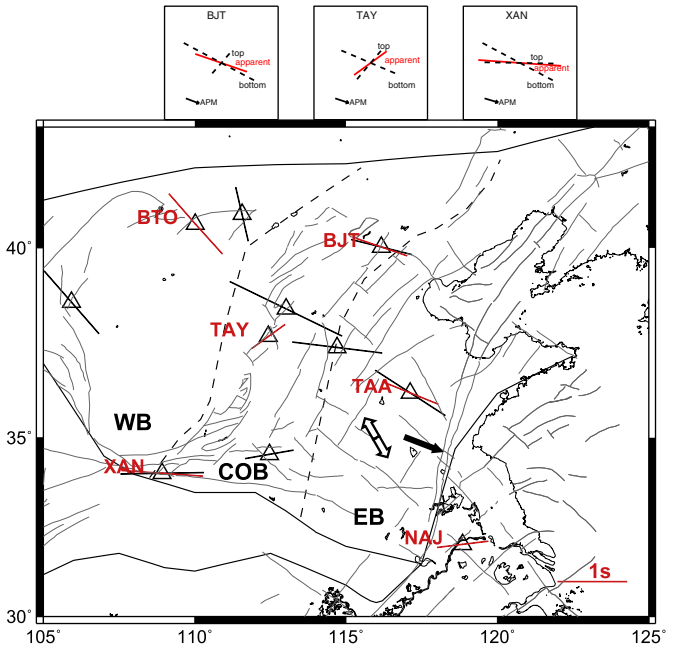

Fig. 5. (Main panel) Comparison of shear-wave splitting results of this study with those of other studies. Red bars with triangles indicate the one-layer splitting results from this study and black bars with triangles indicate those from Luo et al. (2004). The orientation and length of each bar indicate the FPD and the delay time, respectively. Double-headed arrows indicate the regional lithosphere extension direction (Ren et al., 2002). (Top panel) Predicted values of two-layer splitting parameters (broken lines) and one-layer ones (red solid line) for the BJT, TAY, and XAN stations. The local APMs are also shown. For the XAN station, those with fixed-bottom-layer parameters are shown. Other symbols are the same as those in Fig. 1.

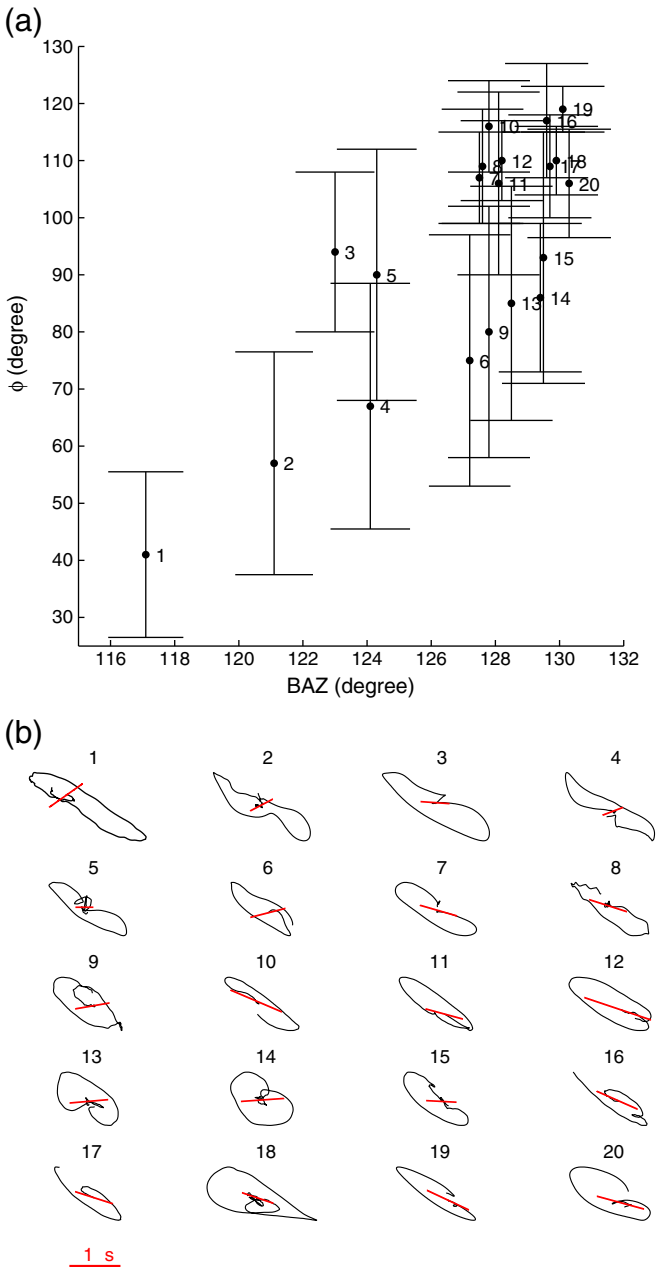

Fig. 6. (a) Apparent FPD as a function of BAZ for 20 events recorded at the BJT station. (b) Particle motions of the SKS phase on NS (vertical axis) and EW (horizontal axis) components. Red bars, which indicate the FPD and the delay time, are drawn by centering on the initial points of the particle motions.

sampling iterations are used to obtain reliable standard errors. The two-layer parameters are shown in the top panel of Fig. 5 and the model prediction with 95% confidence region and the estimated Z misfit are shown in Fig. 7.

The best-estimated FPD of the bottom layer of BJT (118°, Fig. 7(a)) almost coincide with those of TAY (113°, Fig. 7(b)) and XAN (112°, Fig. 7(c)). In the right half of Fig. 7, the misfit function is shown near the best estimates. It is clear that apart from BJT, the delay time of the bottom layer is not well-constrained. Nevertheless, it appears reasonable to grant these values as the estimates for the top layer. Fig. 7(a) shows that the observed variation of the splitting parameters of BJT is quantitatively explained by the two-layer model. The FPD of the bottom layer is at a high angle to the observed apparent FPD but rather close to the direction of the absolute plate motion (APM) of the study area (N111°E ± 5° in the no-net-rotation reference frame for several plate motion models, calculated at website http://sps.unavco.org/). As the regional scale of the APM is nearly a constant, there would be little or no variation in the splitting parameters associated with the asthenospheric flow. By keeping the bottom layer constant as the bottom layer of BJT, we then try to apply the two-layer method to XAN, in which the estimated delay time of the bottom layer is much smaller than that at BJT station. The resulting parameters for this case are shown in Fig. 7(d).

Table 3
Stations used for shear-wave splitting analysis and their final results.

No.	Station	λE/°	φN/°	H/km	ϕ/°	−2σϕ/°	2σϕ/°	δt/s	−2σδt/s	2σδt/s	n
1	BTO	110.0183	40.5983	1.1200	138	−7	12	1.16	−0.24	0.24	4
2	TAY	112.4342	37.7173	0.8500	54	−3	3	0.58	−0.06	0.06	22
3	TAA	117.1244	36.2114	0.3000	112	−3	2	0.86	−0.14	0.10	6
4	NAJ	118.8544	32.0517	0.0450	83	−20	21	0.74	−0.30	0.30	2
5	BJT	116.1679	40.0183	0.1970	109	−3	2	0.78	−0.08	0.12	23
6	XAN	108.9237	34.0313	0.6300	94	−1	1	1.18	−0.06	0.08	29

λ_E, φ_N, and H are the longitude, latitude, and altitude of stations, respectively. ϕ and δt are the fast polarization direction and delay time with 2σ error bars, respectively, and n is the stacked number of records for each station. For simplicity, the range is given as $0° \le \phi \le 180°$ rather than $-90° \le \phi \le 90°$.

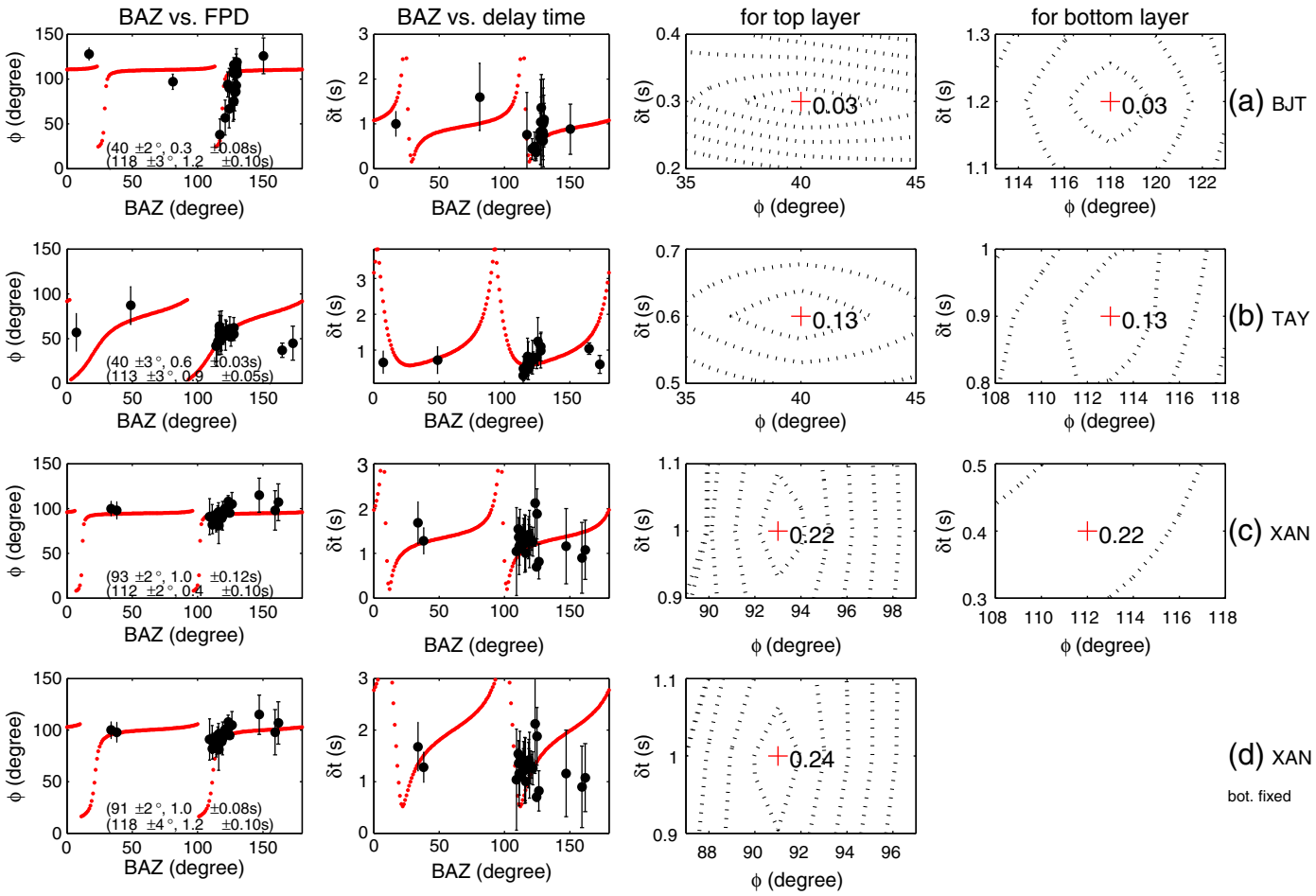

Fig. 7. Results of two layers of anisotropy for (a) BJT, (b) TAY, and (c) XAN stations with no fixed parameters and for (d) XAN station with the same fixed-bottom-layer parameters as those obtained for the BJT station. Red dotted lines show the predicted splitting parameters for a two-layer model with the best-fit parameters indicated in the first column. The third and fourth columns indicate the Z misfit with optimum φ and δt (red crosses) for the top and bottom layers, respectively. Contours are at intervals of 1.

4.2.2. F-test showing significance of two-layer model

We further calculate the F statistic to determine whether the two-layer model gives a significantly better fit to the data than the one-layer model. For each model, we take the weighted sum of squared residuals, Chi-square, for n data points as $X^2_m = \sum_{i=1}^{n}(((\varphi_i - \varphi_i^m)/2\sigma_{\varphi i})^2 + ((\delta t_i - \delta t_i^m)/2\sigma_{\delta ti})^2)$. The F statistic is given by

$$F = \frac{\left(\frac{X^2_{m1} - X^2_{m2}}{p2 - p1}\right)}{\left(\frac{X^2_{m2}}{2*n - p2}\right)}, \quad (1)$$

where one-layer mode ($m1$) and two-layer model ($m2$) have parameters of $p1 = 2$ and $p2 = 4$, respectively. For station BJT, the resulting F statistic is 14.0, which is significantly larger than the critical value 5.2 with the probability of 0.01. We thus are 99% confident that the two-layer model is better than the one-layer model. For station TAY and XAN, the resulting F statistics are small and there are still large misfits between the two-layer model and the data.

4.2.3. Synthetic examples of two layers

To visually inspect the effect of two layers of anisotropy on seismic data, we generate sinusoid-based synthetic seismograms with a period of 8 s; this is the typical dominant period of the seismic waves we used. Fig. 8 shows such doubly split shear waves with splitting parameters obtained for the BJT station. A comparison of this figure with Fig. 6(b) shows that the polarization directions are simulated well. The synthetics exhibit an increasing feature on the NS/EW energy ration with respect to the increasing BAZs. This feature is also detected in observations, except for events 10 and 14, which do not exhibit an increasing trend in the PFDs over the BAZs (see Fig. 6(a)); this may be due to some local structural complexity that has not been modeled here.

5. Discussion

Assuming a mean mantle shear-wave velocity of 4.6 km/s with a typical anisotropy of 4%, the observed values of delay time range from 0.58 s to 1.18 s, corresponding to thicknesses of 67 km to 136 km for the anisotropic layer. With the Moho depth of 31–33 km in eastern China (Chen et al., 2010), the crustal contribution may be less than the average value of 0.2 s. In addition, no obvious anisotropy is found in the lower mantle beneath eastern China (Niu and Perez, 2004). These studies suggest that the observed seismic anisotropy likely lie in the uppermost mantle.

For the COB, a one-layer model is in disagreement with the observed azimuth-dependent splitting parameters; two layers of anisotropy do improve the fit to the data. The result of the two-layer model is shown in the top of Fig. 5; the BJT and TAY stations have FPDs of the bottom layer subparallel to the direction of the APM, indicating the presence of an asthenospheric source for the anisotropy. For the

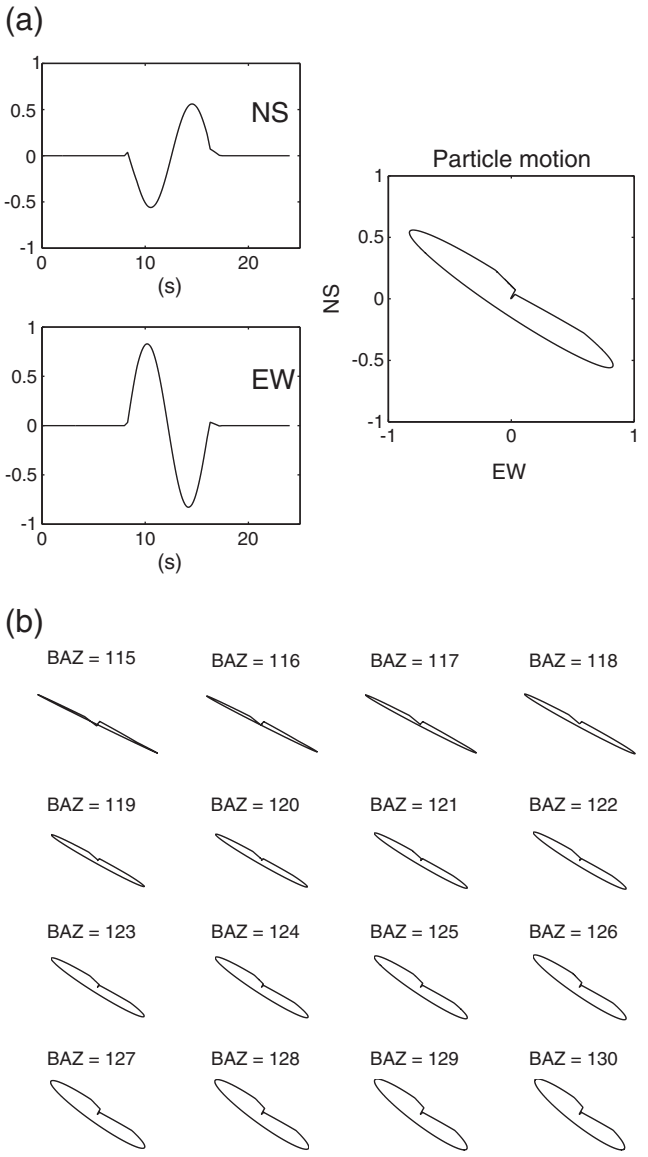

Fig. 8. (a) Synthetic data consisting of one cycle of a sinusoid with a period of 8 s on NS and EW components, which has been split twice using splitting parameters $\varphi 1 = 118°$, $\delta t1 = 1.2$ s, $\varphi 2 = 40°$, and $\delta t2 = 0.3$ s for BAZ = 125°. (b) Same synthetic particle motions for NS and EW components with BAZ ranging from 115° to 130°.

top layer, their FPDs are consistent with the local strikes of the surface faults, suggesting the combined influence of the past orogenies in the lithosphere. A noticeable misfit between the observed and the calculated delay time over the range from 140° to 170° is observed in Fig. 7(d). This may indicate that in the southern margin of the NNC, where a transition occurs from the stable craton to an active deformation in the Qinling belt, the two-layer model is insufficient.

For the EB, the interpretation of the observed anisotropy is non-unique. The NNW–SSE trending lithosphere extension was widespread in the EB during the Late Mesozoic and Cenozoic (Ren et al., 2002). The possible origination of either from the asthenosphere or from the "frozen-in" lithosphere cannot be ruled out on the basis of current observational evidence. However, the observed splitting parameters of TAA (112°) are more identical to the estimated values of the bottom layer of BJT (118°) than that of the regional lithosphere extension direction (~155°). In addition, the extension was suggested to be a shallow feature and not sufficiently strong (Deng et al., 2003) to cause significant anisotropy in teleseismic shear waves. It is more likely that the anisotropy in the EB mainly presents the current strain within the subcratonic asthenosphere related to the interactions between the surrounding plates. It is notable that the azimuthal coverage of available data is still not sufficient, partly because we have employed very strict criteria in selecting the data.

Based on these observations, we may infer that under the EB, the splitting might be mainly controlled by the subcratonic asthenosphere but under the COB, it might be a combination of the lithosphere and asthenosphere. Significant variation of thickness of the lithosphere from the COB of 80–180 km towards the EB of 60–90 km has been revealed by previous studies (e.g., Chen, 2009). This observation supports our proposed model and suggests the complexity in deep structure of the COB. Thus far, two layers of differing anisotropic properties have been quantitatively detected at a few stations worldwide. The observation for the NNC may be regarded as a new line of study for exploring the mantle structure.

Acknowledgements

We are grateful to T. Iidaka and Y. Ishikawa for the useful discussions. Constructive comments are due to editor M. Liu and two anonymous reviewers. The topographic data were obtained from the National Geophysical Data Center. GMT was used for creating some of the figures. LB thanks to the Japan Society for the Promotion of Science (JSPS) for the Research Fellowship. This work is partly supported by Grant-in-Aid for Scientific Research 19104011.

References

Bai, L., Iidaka, T., Kawakatsu, H., Morita, Y., Dzung, N.Q., 2009. Upper mantle anisotropy beneath Indochina block and adjacent regions from shear wave splitting analysis of Vietnam array data. Phys. Earth Planet Inter. 176, 33–43, doi:10.1016/j.pepi.2009.03.008.
Chen, L., 2009. Lithospheric structure variations between the eastern and central North China Craton from S-and P-receiver function migration. Phys. Earth Planet. Inter. 173, 216–227.
Chen, Y.L., Niu, F.L., Liu, R.F., Huang, Z.B., Tkalčić, H., Sun, L., Chan, W., 2010. Crustal structure beneath China from receiver function analysis. J. Geophys. Res. 115, B03307, doi:10.1029/2009JB006386.
Deng, Q.D., Zhang, P.Z., Ran, Y.K., Yang, X.P., Min, W., Chu, Q.Z., 2003. Basic characteristics of active tectonics of China. Sci. China, Ser. D Earth Sci. 46 (4), 356–372.
Earthquake Defence Department, China Earthquake Administration, 1999. The catalogue of modern earthquake catalog in China (A.D.1912~A.D.1990, Ms≥4.7). Science and Technology Press, Beijing: China. 637pp (in Chinese).
Efron, B., 1979. Bootstrap methods: another look at the jackknife. Ann. Stat. 7, 1–26.
Huang, Z.X., Su, W., Peng, Y.J., Zheng, Y.J., Li, H.Y., 2003. Rayleigh wave tomography of China and adjacent regions. J. Geophys. Res. 108 (B2), 2073, doi:10.1029/2001JB001696.
Huang, Z.C., Xu, M.J., Wang, L.S., Mi, N., Yu, D., Li, H., 2008. Shear wave splitting in the southern margin of the Ordos Block, north China. Geophys. Res. Lett. 35, L19301, doi:10.1029/2008GL035188.
Iidaka, T., Niu, F.L., 2001. Mantle and crust anisotropy in the eastern China region inferred from waveform splitting of SKS and PpSms. Earth Planet. Space 53, 159–168.
Kennett, B.L.N., Engdahl, E.R., 1991. Travel times for global earthquake location and phase identification. Geophys. J. Int. 105, 429–465.
Kusky, T.M., Li, J.H., 2003. Paleoproterozoic tectonic evolution of the North China Craton. J. Asian Earth Sci. 22 (4), 383–397.
Liu, X.Q., Zhou, H.L., Li, H., Ji, A.D., 2001. Anisotropy of the upper mantle in Chinese mainland and its vicinity. Acta Seismol. Sin. 23, 337–346 (in Chinese).
Liu, K.H., Gao, S.S., Gao, Y., Wu, J., 2008. Shear wave splitting and mantle flow associated with the deflected Pacific slab beneath northeast Asia. J. Geophys. Res. 113, B01305.
Luo, Y., Huang, Z.X., Peng, Y.J., Zheng, Y.J., 2004. A study on SKS wave splitting beneath the China mainland and adjacent regions. Chin. J. Geophys. 47, 916–926.
Morita, Y., Kanazawa, T., OHP observation groups, 1999. Master plan of OHP joint geophysical observation at the ocean bottom and Chinese continent, Abstract of Joint Meeting of Earth and Planetary Science of Japan, DeP009.
Niu, F., Perez, A.M., 2004. Seismic anisotropy in the lower mantle: a comparison of waveform splitting of SKS and SKKS. Geophys. Res. Lett. 31, L24612.
Ren, J., Tamaki, K., Li, S.T., Zhang, J.X., 2002. Late Mesozoic and Cenozoic rifting and its dynamic setting in Eastern China and adjacent areas. Tectonophys 344, 175–205.
Silver, P.G., Chan, W.W., 1991. Shear wave splitting and subcontinental mantle deformation. J. Geophys. Res. 96, 16429–16454.
Silver, P.G., Savage, M.K., 1994. The interpretation of shear-wave splitting parameters in the presence of two anisotropic layers. Geophys. J. Int. 119, 949–963.

Snyder, D.B., Bostock, M.G., Lockhart, G.D., 2003. Two anisotropic layers in the Slave craton. Lithos 71, 529–539.
Wang, Q., Zhang, P., Freymueller, J.T., Bilham, R., Larson, K.M., Lai, X., You, X., Niu, Z., Wu, J., Li, Y., Liu, J., Yang, Z., Chen, Q., 2001. Present-day crustal deformation in China constrained by Global Positioning System measurements. Science 294, 574–577.
Wolfe, C.J., Silver, P.G., 1998. Seismic anisotropy of oceanic upper mantle: shear-wave splitting observations and methodologies. J. Geophys. Res. 103, 749–771.
Zhao, L., Zheng, T.Y., 2005. Using shear wave splitting measurements to investigate the upper mantle anisotropy beneath the North China craton: distinct variation from east to west. Geophys. Res. Lett. 32, L10309.
Zhao, L., Zheng, T.Y., Chen, L., Tang, Q.S., 2007. Shear wave splitting in eastern and Central China: implications for upper mantle deformation beneath continental margin. Phys. Earth Planet. Inter. 162, 73–84.